

# Single production of fourth-family quarks at the LHC

O. Çakır<sup>1,2,a</sup>, İ.T. Çakır<sup>1</sup>, H. Duran Yıldız<sup>3</sup>, R. Mehdiyev<sup>4,5</sup>

<sup>1</sup>Department of Physics, Theory Division, CERN, 1211 Geneva 23, Switzerland

<sup>2</sup>Faculty of Sciences, Department of Physics, Ankara University, 06100, Tandoğan, Ankara, Turkey

<sup>3</sup>Faculty of Art and Sciences, Department of Physics, Dumluşpınar University, Central Campus, Kütahya, Turkey

<sup>4</sup>Department of Physics, University of Texas at Austin, Austin, TX 78712-0264, USA

<sup>5</sup>Institute of Physics, Azerbaijan National Academy of Sciences, 370143, Baku, Azerbaijan

Received: 30 June 2008 / Published online: 19 August 2008  
© Springer-Verlag / Società Italiana di Fisica 2008

**Abstract** We study the single production of fourth-family quarks through the process  $pp \rightarrow Q'jX$  at the Large Hadron Collider (LHC). We have calculated the decay widths and branching ratios of the fourth-family quarks ( $b'$  and  $t'$ ) in the mass range 300–800 GeV. The cross sections for the signal and background processes have been calculated in a Monte Carlo framework. It is shown that the LHC can discover single  $t'$  and  $b'$  quarks if the CKM matrix elements  $|V_{t'q}|$ ,  $|V_{qb'}| \gtrsim 0.01$ .

## 1 Introduction

The standard model (SM) of the electroweak and color interactions does not predict the number of fermion families. However, due to the limits coming from strong coupling in QCD, the number of quark flavors should be less than eighteen. The electroweak precision measurements done by LEP experiments imply that the number of light neutrinos is equal to three [1]. The replications of three quark and lepton families remain a mystery as part of the flavor problem. A possible fourth family may play a crucial role in our understanding of the flavor structure of the standard theory. The experiments at Tevatron have already constrained the masses of fourth-family quarks. The CDF has the strongest bound on the mass of the  $t'$  quark, being  $m_{t'} > 258$  GeV at 95% CL [2]. This analysis applies to  $t'$  pair production independent of the CKM matrix elements  $V_{t'q}$ . In particular, CDF obtains a bound on the mass of the  $b'$  quark of  $m_{b'} > 268$  GeV [3], taking  $\text{BR}(b' \rightarrow bZ) = 1$ . A recent reexamination of the bounds on the masses of the fourth-family quarks assumes  $m_{Q'} > 255$  GeV [4]. There exists some parameter space (mass-mixing angle) of the fourth-family quarks which could be explored at future collider

searches. The upcoming experiments at the Large Hadron Collider (LHC) are able to probe heavy quarks up to a heavier mass range, accessible to future experiments. Recently, the pair production signals have been considered in [5–7] with a mass range similar to what we consider here. Because of the uncertainties on the CKM matrix elements, there still remains a door open for the fourth-family quarks and their mixings with the other three families. Recent electroweak precision analysis of the S and T parameter also supports the idea of the existence of the fourth-family quarks [8].

A prediction for the fourth-family fermion masses as well as the CKM mixings has been presented in [9, 10]. Pair production of the fourth SM family quarks has been studied at the LHC [11, 12]. Recently, an update has been made on the analysis of the signal and background for the pair production of fourth-family quarks within the ATLAS detector [13].

In this paper, we study the single production (less studied compared to pair production) of the fourth-family quarks through the process  $pp \rightarrow b'(\bar{b}')jX$  and  $pp \rightarrow t'(\bar{t}')jX$  at the LHC. We have calculated the cross sections of signals and corresponding backgrounds in the Monte Carlo (MC) framework. The decay widths and branching ratios of the fourth-family quarks ( $b'$  and  $t'$ ) are calculated in the mass range 300–800 GeV. We analyze the potential of the LHC for probing the fourth-family quarks providing three different parametrizations of the CKM matrix elements  $|V_{t'q}|$  and  $|V_{qb'}|$ .

## 2 Interaction Lagrangian with fourth-family quarks

In the standard model of the electroweak interactions, quarks can couple to charged weak currents by the exchange of a  $W^\pm$  boson and neutral weak currents by the  $Z^0$  boson. The left-handed (right-handed) quark fields transform as doublets (singlets) under the group  $SU(2)$ . We consider an enlarged framework of the SM to include fourth-

<sup>a</sup> e-mail: [ocakir@science.ankara.edu.tr](mailto:ocakir@science.ankara.edu.tr)

family quarks. The interaction of the fourth-family quarks  $Q'_i(t', b')$  and the quarks  $q_i$  via the SM gauge bosons ( $\gamma, g, Z^0, W^\pm$ ) is given by

$$\begin{aligned} L = & -g_e \sum_{Q'_i=b', t'}^4 Q_{ei} \bar{Q}'_i \gamma^\mu Q'_i A_\mu \\ & -g_s \sum_{Q'_i=b', t'} \bar{Q}'_i T^a \gamma^\mu Q'_i G_\mu^a \\ & -\frac{g}{2 \cos \theta_W} \sum_{Q'_i=b', t'} \bar{Q}'_i \gamma^\mu (g_V^i - g_A^i \gamma^5) Q'_i Z_\mu^0 \\ & -\frac{g}{2\sqrt{2}} \sum_{Q'_{j \neq i}=b', t'} V_{ij} \bar{Q}'_i \gamma^\mu (1 - \gamma^5) q_j W_\mu^\pm, \end{aligned} \quad (1)$$

where  $g_e, g$  are electroweak coupling constants, and  $g_s$  is the QCD coupling constant.  $A_\mu, G_\mu, Z_\mu^0$  and  $W_\mu^\pm$  are the vector fields for photon, gluon,  $Z^0$  boson and  $W^\pm$  boson, respectively.  $Q_{ei}$  is the electric charge of the fourth-family quarks;  $T^a$  are the Gell-Mann matrices.  $g_V$  and  $g_A$  are the vector and axial-vector type couplings of the neutral weak current. Finally,  $\mathbf{V} = Y^{u\dagger} Y^d$  (where  $Y^{u,d}$  is for the Yukawa couplings) is the corresponding  $4 \times 4$  CKM matrix:

$$\mathbf{V} = \begin{pmatrix} V_{ud} & V_{us} & V_{ub} & V_{ub'} \\ V_{cd} & V_{cs} & V_{cb} & V_{cb'} \\ V_{td} & V_{ts} & V_{tb} & V_{tb'} \\ V_{t'd} & V_{t's} & V_{t'b} & V_{t'b'} \end{pmatrix}. \quad (2)$$

The constraint on the mixing between the quarks comes from the unitarity of the CKM matrix in the SM. These constraints appear to be well satisfied experimentally for the three-family case and the elements of the  $3 \times 3$  submatrix are well tested by various processes [1]. The elements in the fourth row and column are constrained by flavor physics, and the flavor changing neutral current (FCNC) effects are suppressed by the Glashow–Iliopoulos–Maiani (GIM) mechanism. The  $4 \times 4$  quark mixing matrix  $\mathbf{V}$  satisfies the unitarity conditions,

$$\sum_{\alpha=1}^4 |V_{i\alpha}|^2 = \sum_{j=1}^4 |V_{j\beta}|^2 = 1 \quad (3)$$

for  $i, j = u, c, t, t'$  and  $\alpha, \beta = d, s, b, b'$ . In addition to these constraints, if the following constraints are also satisfied:

$$\sum_{\alpha=1}^4 V_{i\alpha} V_{j\alpha}^* = \sum_{j=1}^4 V_{j\alpha} V_{j\beta}^* = 0 \quad (4)$$

for all indices ( $i \neq j$  in the first sum and  $\alpha \neq \beta$  in the second sum), the triangles will have the same areas. The first, second and third rows of the matrix  $\mathbf{V}$  with the measurement from currently available experiments can be calculated to be  $|V_{ub'}|^2 = 0.0008 \pm 0.0011$ ,  $|V_{cb'}|^2 = 0.0295 \pm 0.1780$  and  $|V_{tb'}|^2 = 0.4054 \pm 0.3696$ . For the first three columns we calculate  $|V_{t'd}|^2 = -0.001 \pm 0.005$ ,  $|V_{t's}|^2 = 0.0315 \pm 0.1780$  and  $|V_{t'b}|^2 = 0.4053 \pm 0.3696$ . The mixing between the third and fourth family is less constrained. A lower limit can be obtained from the single production of top quarks, such as  $|V_{tb}| > 0.68$  at 95% C.L. [14, 15]. If there is a mass degeneracy between the  $b'$  and  $t'$  quarks, two body decay occurs mostly into third generation quarks via charged currents.

### 3 Production cross section

The fourth-family quarks  $b'$  and  $t'$  can be produced singly at the LHC. There are the processes  $q\bar{q} \rightarrow Q'\bar{q}'$ ,  $qq' \rightarrow Q'q''$  and  $q\bar{q}' \rightarrow Q'\bar{q}''$  relevant for single production as shown in Fig. 1. As can be seen from (1) and Fig. 1 the single production cross section strongly depends on the CKM elements  $V_{qb'}$  or  $V_{t'q}$ . The cross sections for the subprocesses in Fig. 1 are summed to make a “ $Q' + jet$ ” analysis in the final state. The total cross section for the process  $pp \rightarrow Q'jX$  is expressed by

$$\sigma = \sum_{i,j} \int_{y_{\min}}^1 dy \int_y^1 \frac{dx}{x} f_{q_i/p}(x, Q^2) f_{q_j/p}(y/x, Q^2) \hat{\sigma}(ys), \quad (5)$$

where the lower limit of the first integral is chosen to be  $y_{\min} = m_{Q'}^2/s$ . The parton distribution function (PDF)  $f_{q/p}(x, Q^2)$  is taken from the CTEQ6M [16] with  $Q^2 = m_{Q'}^2$  for the signal and  $Q^2 = \hat{s}$  for the background. In order to compare the magnitude of the single production cross

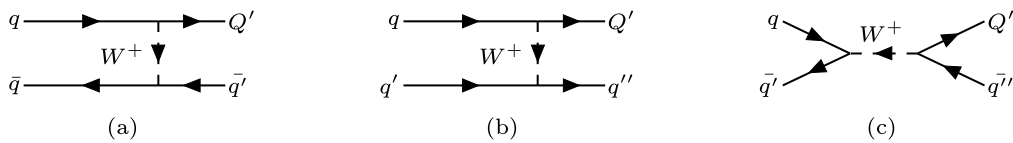


**Fig. 1** The diagrams for single production of fourth-family quarks

section with the pair production, we plot in Fig. 2 the dependence on the mass of the fourth-family quarks. The pair production of fourth-family quarks at the LHC is mainly due to gluon–gluon fusion and quark–antiquark annihilation processes [13]. In addition, there is also a contribution from  $W$  boson exchange in the  $t$ -channel when the CKM matrix elements  $V_{t'q}$ ,  $V_{qb'}$  are taken large. The relevant diagrams are shown in Fig. 3. We use three parametrizations, called PI, PII and PIII for the CKM elements corresponding to  $V_{Q'i} = V_{iQ'} = 0.01$ ,  $V_{Q'i} = V_{iQ'} = 0.05$  and  $V_{ub'} = 0.044$ ,  $V_{cb'} = 0.46$ ,  $V_{td} = 0.063$ ,  $V_{ts} = 0.46$ ,  $V_{tb} = 0.47$ , respectively. The reason for choosing these options is that only

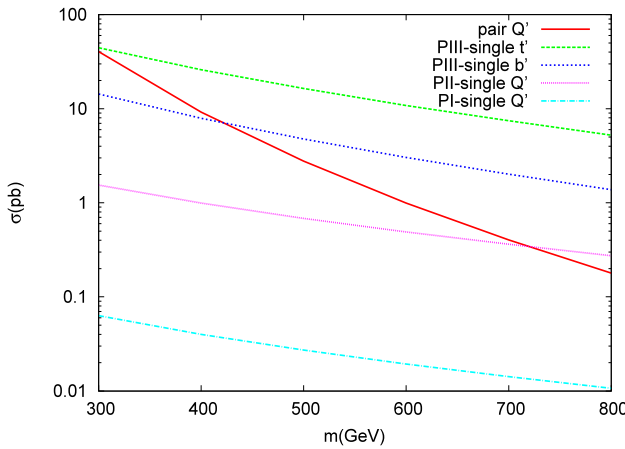
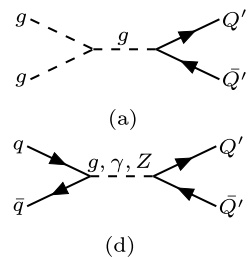


**Fig. 2** The cross sections for the single and pair production of  $b'$  and  $t'$  quarks at LHC for different parametrizations of the CKM matrix elements  $V_{t'q}$  and  $V_{qb'}$

**Fig. 3** The diagrams for the pair production of fourth-family quarks through gluon–gluon fusion and quark–antiquark annihilation processes



the upper limits on the CKM elements could be well predicted from the current experimental data, and they can be relaxed as  $1\sigma$  over the average values. For a parametrization with equal strengths,  $V_{iQ'} = V_{Q'i}$ , the single production cross section becomes comparable to the pair production cross section for the value of the CKM matrix elements  $V_{t'q}$ ,  $V_{qb'} = 0.25–0.04$  in the mass range  $m_{Q'} = 300–800$  GeV, as shown in Fig. 2. The cross section for single  $t'$  and  $b'$  production is almost the same for the parametrization PI and PII in the mass range of interest.

The decay channels of fourth-family quarks are strongly related to the non-diagonal matrix elements  $V_{t'q}$ ,  $V_{qb'}$  and the diagonal  $V_{tb'}$ . The production cross section in dependence on the mass of the fourth-family quarks is given in Table 1 for the parametrizations PI–PIII. These values are obtained by using CalcHEP program [17, 18]. In the first and second parametrizations the cross sections are low, as expected from the fact that the single production cross section simply scales with  $|V_{t'q}|^2$  and  $|V_{qb'}|^2$ . All the related vertices are implemented into the program and the model files can be found at [19]. In order to compare the range of the error in the cross sections coming from the source of the parton distributions CTEQ6L and CTEQ6M at  $Q^2 = m_{Q'}^2$ , we present the total cross section in Table 2 for single and pair production of the fourth-family quarks at the LHC. As can be seen from this table, the relative difference in pair production is higher than in the single production mechanism. The single production cross sections differ by about 10% at  $m_{Q'} = 300$  GeV for two options of CTEQ distribution, while pair production differs at most  $\sim 18\%$ . For

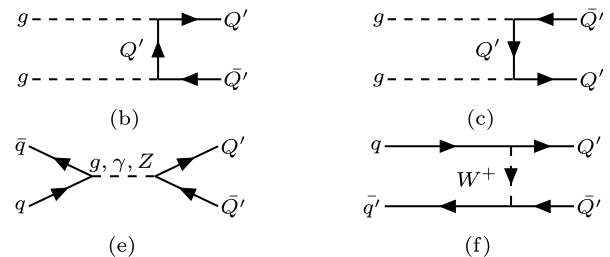


**Table 1** The cross section in pb for single production of the fourth-family quarks  $b'(\bar{b}')$  and  $t'(\bar{t}')$  at the LHC. The parametrizations PI–PIII are explained in the text. The numbers in the parentheses denote the antiparticle case. Here, we have used CTEQ6M at the scale  $Q^2 = m_{Q'}^2$

Process →	$pp \rightarrow b'(\bar{b}')jX$			$pp \rightarrow t'(\bar{t}')jX$		
	Mass (GeV)	PI	PII	PIII	PI	PII
300	0.06(0.02)	1.54(0.62)	14.34(20.31)	0.06(0.02)	1.58(0.58)	44.56(25.70)
400	0.04(0.02)	0.99(0.37)	7.95(11.77)	0.04(0.01)	1.00(0.33)	26.06(14.44)
500	0.03(0.01)	0.68(0.23)	4.77(7.31)	0.03(0.01)	0.68(0.20)	16.36(8.75)
600	0.02(0.01)	0.49(0.15)	3.03(4.78)	0.02(0.01)	0.48(0.13)	10.82(5.59)
700	0.01(0.004)	0.36(0.11)	2.01(3.24)	0.01(0.003)	0.35(0.09)	7.42(3.71)
800	0.01(0.003)	0.27(0.08)	1.38(2.26)	0.01(0.002)	0.27(0.06)	5.25(2.54)

**Table 2** The total cross section in pb for pair production of the fourth-family quarks  $Q'$  at the LHC. The values are given for two options of the parton distribution function CTEQ6 with  $Q^2 = m_{Q'}^2$

$Q^2 = m_{Q'}^2$ Mass (GeV)	$pp \rightarrow Q' j X(\text{PI})$		$pp \rightarrow Q' \bar{Q}' X(\text{PI})$	
	CTEQ6L	CTEQ6M	CTEQ6L	CTEQ6M
300	0.06	0.06	34.34	40.36
400	0.04	0.04	7.63	9.21
500	0.03	0.03	2.27	2.77
600	0.02	0.02	0.82	0.99
700	0.01	0.01	0.33	0.40
800	0.01	0.01	0.15	0.18

higher mass values the difference between the two choices gets smaller. The ratios  $\sigma(pp \rightarrow t' j X)/\sigma(pp \rightarrow tj X)$  and  $\sigma(pp \rightarrow t' \bar{t}' X)/\sigma(pp \rightarrow t \bar{t} X)$  can also be used to reduce the uncertainties from the PDFs. The cross sections for the single and pair production of top quarks at the LHC are 140.94 pb for single production and 492.36 pb for pair production when the CTEQ6L is used at the scale  $Q^2 = m_t^2$ .

#### 4 Decay widths and branchings

If  $m_{t'} > m_{b'}$ , then  $t'$  and  $b'$  quarks can decay as

$$\begin{aligned} t' &\rightarrow W^+ b' \\ &\rightarrow W^+ b \quad b' \rightarrow W^- t \\ &\rightarrow W^+ q(d, s), \quad \rightarrow W^- q(u, c). \end{aligned} \quad (6)$$

If  $m_{b'} > m_{t'}$ , the  $b'$  and  $t'$  quarks can decay as follows:

$$\begin{aligned} b' &\rightarrow W^- t' \\ &\rightarrow W^- t \quad t' \rightarrow W^+ b \\ &\rightarrow W^- q(u, c), \quad \rightarrow W^+ q(d, s). \end{aligned} \quad (7)$$

In the first lines of (6) and (7), two body decay  $Q'_i \rightarrow Q'_j + W^\pm$  takes place with a virtual (real)  $W$  boson depending on the mass difference  $|m_{t'} - m_{b'}| \lesssim 80 (> 80)$  GeV. In the analysis, both two body decays and three body decays (via a virtual  $W^{\pm*}$  boson) are considered. Fourth-family quarks will decay into third-family quarks associated with a  $W^\pm$  boson as shown in the second line of (6) and (7). The last lines of the above equations denote the fourth-family quark decays into light jets.

The branching ratios for the  $b'$  decays according to the PIII parametrization are given in Table 3. As can be seen from this table, the fractions are dominant for the  $b' \rightarrow W^- c$  and  $b' \rightarrow W^- t$  channels. For the other parametrization, the branchings change slightly in the mass range of interest, for example:  $\text{BR}(b' \rightarrow W^- u(c)) = 36.6(33.4)\%$  and  $\text{BR}(b' \rightarrow W^- t) = 26.9(33.3)\%$  at  $m_{b'} = 300(800)$  GeV.

**Table 3** The branching ratio (%) for the  $b'$  decays according to the parametrization PIII. For the other parametrizations, PI and PII, the branchings' change is very small in the considered mass range

Mass (GeV)	$W^- u$	$W^- c$	$W^- t$
300	0.5	56.3	43.2
400	0.5	50.2	49.3
500	0.5	50.3	49.2
600	0.5	48.9	50.6
700	0.5	48.8	50.7
800	0.4	48.8	50.8

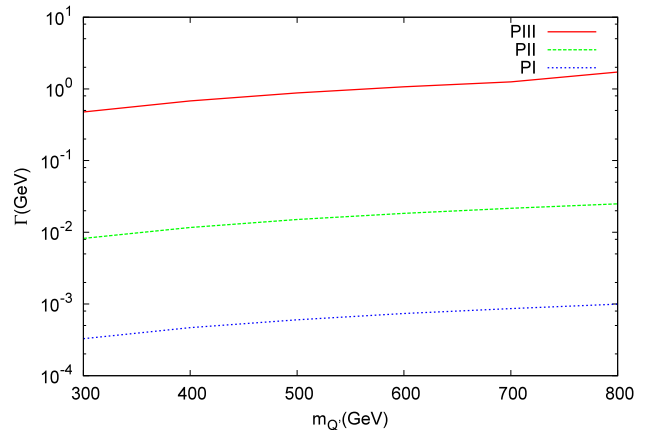


**Fig. 4** Decay width of the fourth-family quarks for the parametrizations PI–PIII

Concerning the options PI and PII, the  $t'$  branchings  $\text{BR}(t' \rightarrow W^+ q) = 33.3\%$  remain the same for all channels in the considered mass range, while they are 51% ( $W^+ b$ ), 48% ( $W^+ s$ ) and 1% ( $W^+ d$ ) for option PIII. In Table 3, the  $b'$  decay modes and fractions are displayed. We have used these modes and fractions in order to calculate the statistical significances (SS) as explained in the next section.

In the case of mass degeneracy,  $m_{t'} = m_{b'}$ , both the  $t'$  and the  $b'$  quark decays into SM three-family quarks with a charged current interaction. The total decay widths, depending on the mass, are given in Fig. 4 for the three parametrizations PI–PIII of the CKM matrix elements. The total widths are smoothly increasing with increasing masses. Option PIII has the highest total widths among the other options, PI and PII. For example, at PIII with  $m_{Q'} = 700$  GeV the decay width is  $\Gamma_{Q'} = 1.5$  GeV, which is comparable to that of the top quark.

#### 5 Signal and background

The signal which we consider here for  $t'$  and  $b'$  single production includes the decay chains  $t' \rightarrow W^+ b \rightarrow l^+ \nu_l b$  (or

**Table 4** The cross section in pb for the background relevant to the single  $b'(\bar{b}')$  and  $t'(\bar{t}')$  productions as discussed in the text. The results are given for the backgrounds including two and three weak bosons in the final state

Background	$\sigma (pb)$
$ZZZ$	$1.111 \times 10^{-2}$
$ZZW^+$	$2.050 \times 10^{-2}$
$ZZW^-$	$1.091 \times 10^{-3}$
$W^+W^-W^+$	$8.826 \times 10^{-2}$
$W^+W^-W^-$	$4.463 \times 10^{-2}$
$W^+W^-Z$	$1.033 \times 10^{-1}$
$W^+Z$	$1.868 \times 10^1$
$W^-Z$	$1.169 \times 10^1$
$W^+W^-$	$8.367 \times 10^1$

$l^+\nu_l j$ ) and  $b' \rightarrow W^-t \rightarrow l^-\bar{\nu}_l l^+\nu_l b$  (or  $l^-\bar{\nu}_l l^+\nu_l j$ ), respectively. The antiparticle  $\bar{t}'$  decays similarly but with an opposite charged lepton in the final state. However,  $b'$  or  $\bar{b}'$  quarks decay eventually into two oppositely charged leptons, and hence they should be taken into account together to enhance the statistics. Since a  $b$ -jet can be identified with good efficiency, we consider  $b$ -jets in the final state. In our calculations we take into account leptonic decays of the  $W$  boson ( $W \rightarrow l\nu_l$ , where  $l = e, \mu$ ). The corresponding backgrounds contain a charged lepton,  $b$ -jet and/or other jets and missing energy for the single  $t'$  production signal; and two oppositely charged leptons,  $b$ -jet and/or other jets and missing energy for the single  $b'$  production signal. We calculate the cross sections for the  $W^\pm Z$ ,  $W^+W^-$ ,  $ZZZ$ ,  $ZZW^\pm$ ,  $W^+W^-Z$ ,  $W^+W^-W^\pm$  and  $Wbj$ ,  $Wtj$  backgrounds. These backgrounds are calculated by using CalcHEP with the PDF CTEQ6M at  $Q^2 = \hat{s}$ . The results are given in Table 4 for the backgrounds including two or three weak bosons. These backgrounds give relatively small cross sections when they are multiplied by the corresponding branching ratios for the channels of interest. The backgrounds including  $Wbj$  and/or  $Wtj$  in the final state need to be studied in detail to see the signal over the background, while the others give relatively smaller cross sections. The background process  $pp \rightarrow WbjX$  includes the single production of top quarks as well. By applying an invariant mass cut on the  $m_{Wb} > 200$  GeV this background can be reduced. The transverse momentum distribution of the final jet for the background processes  $pp \rightarrow WQjX$  is shown in Fig. 5. The  $p_T$  distributions of the jet for  $W^+bj$  and  $W^-\bar{b}j$  backgrounds have a similar shape, while they differ from the backgrounds  $W^+\bar{t}j$  and  $W^-\bar{t}j$ . In order to reduce the relevant backgrounds and preserve the signal, we applied the acceptance cuts  $p_T^j > 20$  GeV for the final state jets. The invariant mass distribution  $m_{WQ}$  is given in Fig. 6. For the invariant mass of interest range the backgrounds  $W^+\bar{t}j$  and  $W^-\bar{t}j$  contribute dominantly. We also apply an invariant mass cut like  $|m_{t'} - m_{W^+b}| < 10\text{--}20$  GeV, depending on the  $t'$  mass, and, similarly,  $|m_{b'} - m_{W^-t}| < 10\text{--}20$  GeV for the  $b'$  signal. In this case, we obtain a significant reduction on the

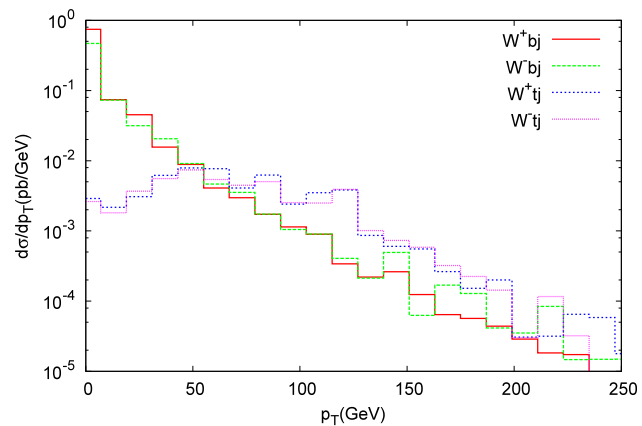


**Fig. 5** The differential cross section depending on the transverse momentum of the final state jet. The solid line (red) and dashed line (green) correspond to the  $W^+bj$  and  $W^-\bar{b}j$  backgrounds, respectively; the dotted and dot-dashed lines refer to the backgrounds  $W^+\bar{t}j$  and  $W^-\bar{t}j$ , respectively

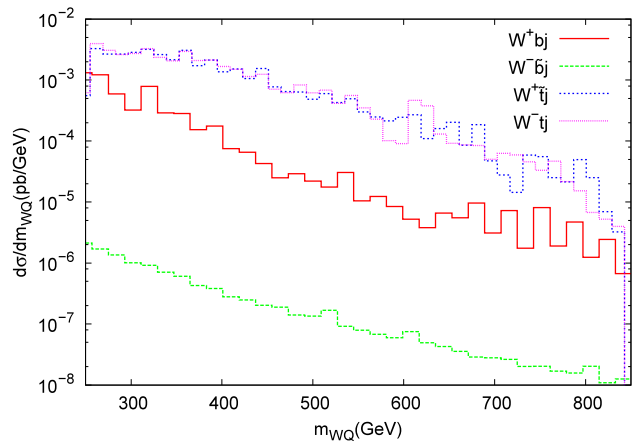


**Fig. 6** Invariant mass distributions for the  $W^\pm Q$  final state, the solid (red) and dashed (green) lines correspond to the  $W^+bj$  and  $W^-\bar{b}j$  backgrounds, while dotted (blue) and dot-dashed (purple) lines correspond to  $W^+\bar{t}j$  and  $W^-\bar{t}j$

cross section of the background as shown in Table 5. The reconstructed invariant mass spectrum,  $m_{Wb}$ , for the  $t'$  signal (where  $m_{t'} = 300$  GeV and 600 GeV) and the corresponding background are given in Fig. 7.

For single  $b'$  production, the main and most demanding background is the  $W^-tj$  process. We applied two different sets of criteria to reduce this background. In the first set, the transverse momentum cut  $p_T^j > 20$  GeV is applied. Applying the transverse momentum cut ( $p_T^j > 50$  GeV), most of the soft jets can be rejected. The latter cut is more efficient than the first one, since with the former cut, some soft jets can still be found. Applying the strict cut ( $p_T^j > 50$  GeV), the reduction efficiency for the background  $W^-tj$  is high enough for the mass range of interest to observe the  $b'$  signal over the background.

For the  $t'$  signal, we consider the  $W^+Z$ ,  $W^-Z$ ,  $W^+W^-$  and  $W^+bj$  reducible backgrounds. These are all reducible backgrounds with respect to the applied cuts. The background cross sections with respect to the applied cuts are displayed in Table 5. Here, the most obstinate background is  $W^+bj$ , which has a cross section of 240 pb before the cuts. It decreases to a reasonable value when we apply the invariant mass and transverse momentum cuts. The background  $W^-\bar{b}j$  is also important for the  $\tilde{t}'$  signal. It should be considered together with the  $W^+bj$  background; possible the asymmetry for producing single  $t'$  and  $\tilde{t}'$  will give additional information. By applying the cuts  $p_T^j > 50$  GeV and choosing the appropriate invariant mass in-

tervals  $\Delta m = |m_{t'} - m_{Wb}|$ , the cross sections for the backgrounds can be reduced below the signal cross section level.

## 6 Signal significance

We define the  $t'(b')$  signal as the final state including a  $b$ -jet or a light jet, a charged lepton (two leptons with opposite sign) and missing transverse momentum. We also require the reconstructed invariant mass distribution  $m_{WQ}$  showing a peak around  $m_{Q'}$  in the interval 300–800 GeV. We can estimate the statistical significance of the signal by using an integrated luminosity of  $L_{\text{int}} = 10^5 \text{ pb}^{-1}$ , which will be achieved in a year run at the LHC. By using the integrated luminosity ( $L_{\text{int}}$ ), signal ( $\sigma_S$ ) and background ( $\sigma_B$ ) cross sections, the branchings  $\text{BR}(Q' \rightarrow WQ)$  followed by  $\text{BR}(W \rightarrow l\nu)$  to the chosen detectable channel, and the relevant efficiency  $\epsilon$  for the signal and background channel, we define the statistical significance (SS) by

$$\text{SS} = \frac{\sigma_S}{\sqrt{\sigma_B}} \sqrt{\epsilon \cdot L_{\text{int}}} \quad (8)$$

In our calculations, the  $b$ -tagging efficiency (60%) and the identification efficiency for each electron (90%) and muon (95%) are taken as reference values based on ATLAS studies [12] for the relevant final states of signal and background. The significances are shown in Table 6 with respect to the fourth-family quark masses in the interval  $m_{Q'} = 300$ –800 GeV for the three parametrizations PI–PIII. In order to calculate the signal significances for all mass ranges (300–800 GeV), one needs to calculate the branching modes and

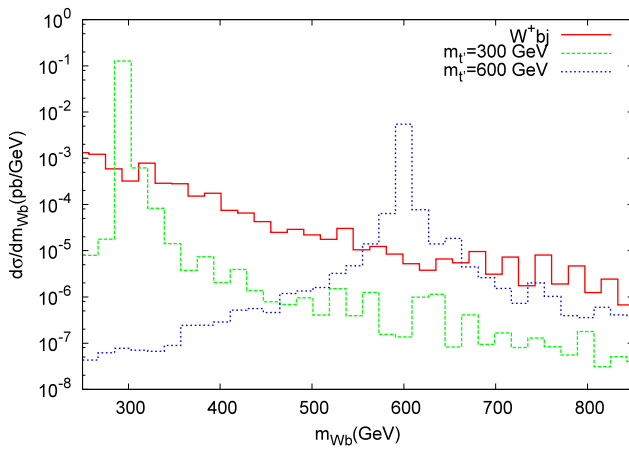


**Fig. 7** The invariant mass distribution for the  $Wb$  signal from  $t'$  decay and the corresponding background

**Table 5** The cross section in pb for  $pp \rightarrow W^-tjX(W^+\bar{t}jX)$  and  $pp \rightarrow W^+bjX(W^-\bar{b}jX)$  background with (w) and without (o) cuts  $p_T^j > 20(50)$  GeV in the various mass ranges of  $\Delta m_{Wt}$  or  $\Delta m_{Wb}$  (numbers shown in the first line are in GeV)

Process	No cut	290–310	390–410	485–515	585–615	680–720	780–820
$pp \rightarrow W^+\bar{t}jX$	9.77	0.44(0.24)	0.20(0.12)	0.13(0.09)	0.07(0.04)	0.05(0.03)	0.03(0.02)
$pp \rightarrow W^-tjX$	11.38	0.42(0.23)	0.21(0.13)	0.14(0.09)	0.07(0.05)	0.05(0.03)	0.02(0.02)
$pp \rightarrow W^+bjX$	240.34	1.37(0.62)	0.28(0.19)	0.21(0.16)	0.12(0.08)	0.05(0.06)	0.05(0.04)
$pp \rightarrow W^-\bar{b}jX$	180.29	0.97(0.43)	0.23(0.18)	0.22(0.16)	0.18(0.12)	0.09(0.09)	0.05(0.02)

**Table 6** Statistical significance (SS) for  $b'(\bar{b}')$  and  $t'(\tilde{t}')$  at the LHC with an integrated luminosity of  $L_{\text{int}} = 10^5 \text{ pb}^{-1}$

SS Mass (GeV)	$b'(\bar{b}')$ quark			$t'(\tilde{t}')$ quark		
	PI	PII	PIII	PI	PII	PIII
300	1.73(0.69)	43.22(17.27)	640.91(892.34)	2.94(1.31)	73.67(32.86)	3184.04(2211.22)
400	1.78(0.67)	44.54(16.78)	544.88(813.12)	3.34(1.17)	83.57(29.22)	3325.72(1928.79)
500	1.49(0.51)	37.45(12.73)	396.28(597.43)	2.49(0.75)	62.26(18.83)	2290.62(1225.12)
600	1.50(0.49)	37.50(12.17)	352.11(561.61)	2.43(0.56)	60.73(14.13)	2079.25(909.39)
700	1.33(0.39)	33.19(9.87)	285.65(453.42)	2.13(0.44)	53.48(11.00)	1707.09(696.92)
800	1.34(0.37)	33.59(9.19)	261.49(416.81)	2.07(0.62)	51.97(15.41)	1559.32(965.05)

fractions, and the associated total width for each mass values with the proposed CKM options P1, PII and PIII. We use the branchings from Table 3 for  $b'$  and almost constant values for  $t'$  together with the signal and the corresponding background cross sections in the chosen invariant mass intervals.

As can be seen from Table 6, in the third option the statistical significances are very high, while the other two options have fairly low values. The lowest  $SS$  values are obtained for the  $t'$  and  $\bar{b}'$  productions in the P1 option. Both the  $b'(\bar{b}')$  and  $t'(\bar{t}')$  signal can be probed at the LHC at the nominal luminosity with greater significances for the parametrization PII and PIII.

As a result, this study shows that, if the fourth-family quarks are present, the LHC will discover them and measure their masses. The single production of fourth-family quarks is very important to measure their mixings with the other families. For the options P1–PIII, the  $t'$  signal will be observed with a significance greater than  $2\sigma$ , if  $V_{t'q}, V_{qb'} \geq 0.01$  for interested mass range. As can be seen from Table 6, the other options, PII and PIII, provide much better significances for the discovery of fourth-family quarks in the mass interval 300–800 GeV.

## 7 Conclusions

This study shows that in the case of the single production of fourth-family  $b'$  and  $t'$  quarks, a mixing down to 1% can be measured at LHC with nominal luminosity, provided that the fourth-family quarks have mass in the range 300–800 GeV. The measurements on  $V_{t'q}$  and  $V_{qb'}$  can also be improved if a possible luminosity upgrade is made at the LHC. In case the fourth-family quarks are present, the LHC will discover them in pairs and measure their masses with a good accuracy. In addition, to obtain mixing of the fourth-family quarks with the other families, the single production of these new quarks remains to be measured. Once the LHC begins to run, the Higgs boson can be found using the golden mode [20, 21] for the relevant mass range. Given the measurements of cross section for Higgs production as well

as the branching ratios of Higgs bosons into possible decay modes, the LHC will be able to verify that the fourth-family quarks do indeed exist. Combining the information from the pair production of fourth-family quarks and their subsequent decays, the single production mechanism may provide a unique measurement of the family mixing with the fourth-family quarks.

**Acknowledgement** This work is supported by the CERN Theory Division. H. Duran Yıldız acknowledges the support from the Turkish State Planning Organization under the grant no. DPT2006K-120470. H. Duran Yıldız's work is also supported by TÜBİTAK under grant no. 105T442.

## References

1. W.-M. Yao et al., J. Phys. G **33**, 1 (2006), <http://pdglive.lbl.gov/>
2. <http://www-cdf.fnal.gov/physics/new/top/2005/ljets/tprime/gen6/public.html>
3. T. Aaltonen et al., CDF Collaboration, Phys. Rev. D **76**, 072006 (2007), <arXiv:hep-ex/0706.3264>
4. P.Q. Hung, M. Sher, <arXiv:0711.4353>
5. B. Holdom, J. High Energy Phys. **0608**, 076 (2006)
6. B. Holdom, J. High Energy Phys. **0703**, 063 (2007)
7. B. Holdom, J. High Energy Phys. **0708**, 069 (2007)
8. G.D. Kribs et al., Phys. Rev. D **76**, 075016 (2007), ANL-HEP-PR-07-39, <arXiv:0706.3718>
9. A. Celikel, A.K. Ciftci, S. Sultansoy, Phys. Lett. B **342**, 257 (1995)
10. S. Atag et al., Phys. Rev. D **54**, 5745 (1996)
11. E. Arik et al., Phys. Rev. D **58**, 117701 (1998)
12. ATLAS Collaboration, ATLAS Detector and Physics Performance Technical Design Report II, ATLAS-TDR-15, CERN-LHCC-99-15, vol. 2, p. 519 (1999)
13. V.E. Ozcan, S. Sultansoy, G. Unel, ATL-COM-PHYS-2007-044
14. V.M. Abazov et al., D0 Collaboration, Phys. Rev. Lett. **98**, 181802 (2007)
15. F. Canelli et al., CDF Collaboration, Conference Note 8588 (2007)
16. J. Pumplin et al., CTEQ Collaboration, <arXiv:hep-ph/0201195>
17. A. Pukhov et al., Preprint INP MSU 98-41/542, <arXiv:hep-ph/9908288>
18. A. Pukhov et al., <hep-ph/0412191>
19. <http://ocakir.web.cern.ch/ocakir/fourthfamily.html>
20. E. Arik et al., Phys. Rev. D **66**, 033003 (2002)
21. E. Arik et al., Eur. Phys. J. C **26**, 9 (2002)